ORIGINAL PAPER

Vibration Control of Electromagnetic Damper System Based on State Observer and Disturbance Compensation

Xian Xu[1,4] · Xiangjun Xia[1] ⬤ · Minyi Zheng[1,2] · Nong Zhang[1,3] · Yuanchang Chen[5]

Abstract
Background Electromagnetic damper (EMD), which is regarded as an emerging type of damper, has drawn wide attention in vibration control fields. One of the main challenges of EMD is the design of controllers, many of which have adopted some unmeasured signals and have ignored the system's disturbance.
Purpose To fill this research gap, a H_∞ controller based on state estimation and disturbance compensation is designed, and an EMD seat suspension system is applied in this research.
Methods A two-degree-of-freedom (DOF) seat suspension and the EMD system models are introduced and established first. Then, the Bouc-Wen model is selected to represent the system's disturbance, including seat suspension friction and the EMD system's inertia force. A test bench is built to measure the system's force-displacement data, and the parameters of the Bouc-Wen model can be determined by parameter identification methods. Secondly, a robust H_∞ controller based on state estimation and disturbance compensation is proposed. A state observer is proposed to estimate unmeasurable state variables and is used in the design of the proposed H_∞ controller. Finally, another test bench, which consists of a six-DOF vibration platform and an EMD seat suspension system, is built. Three typical excitations, sinusoidal, bump, and random excitations, are selected to simulate the real road excitation. A commercial suspension with good vibration isolation capacity is selected to compare with the EMD seat suspension.
Results Experimental results demonstrate that the H_∞ controller can improve vertical ride comfort and reduce suspension deflection effectively.
Conclusion In addition, the designed controller can reduce vibration magnitude in all interested frequency ranges compared with the passive one.

Keywords Electromagnetic damper · State observer · Disturbance compensation · Bouc–Wen model

---

✉ Xiangjun Xia
xx661@uowmail.edu.au

✉ Minyi Zheng
zheng_minyi@hfut.edu.cn

1 School of Automotive and Transportation, Hefei University of Technology, Hefei 230009, China

2 School of Mechanical Engineering, Hefei University of Technology, Hefei 230009, China

3 Automotive Research Institute, Hefei University of Technology, Hefei 230009, China

4 Technology Center of Dongfeng Commercial Vehicle, Dongfeng Commercial Vehicle Co. LTD, Wuhan 430056, China

5 Structural Dynamics and Acoustic Systems Laboratory, University of Massachusetts Lowell One University Avenue, Lowell, MA 01854, USA

Introduction

Severe vibration is one of the main challenges for suspension systems since serious vibration may cause terrible health and safety issues [1]. Seat suspension is widely used to isolate uneven road vibration and provide good ride comfort to drivers, passengers, and cargo [2]. The seat suspension system can be categorized into passive, semi-active, and active seat suspension [3]. Traditional passive seat suspensions have been adopted in many kinds of vehicles and have been studied widely for their simple structure and low cost. However, passive seat suspensions cannot provide good vibration isolation performance at all frequencies considered because of their fixed stiffness and damping parameters [4, 5].

To improve vibration suppression performance further, intelligent suspensions, including active and semi-active

suspensions, have been applied to seat suspensions. Some intelligent materials are used in the design of semi-active suspensions due to their fast response speed, good controllability, and large force output range. The most common semi-active magnetorheological (MR) suspensions have been used in seats and achieved good performance [6–8]. However, the cost of intelligent materials is still high and obstructs their actual application.

Compared with semi-active seat suspensions, active seat suspensions usually have better comprehensive performance because active suspensions can provide ideal controllable force. There are two research hotspots of active seat suspensions: actuator design and control algorithms. Reputable control algorithms, such as robust control [9], neural network control [10], PID control [11], fuzzy control [12–14], sliding mode control [15, 16] and event-triggered control [17–19], have been adopted in seat suspensions in recent years. Although active seat suspensions have better performance than semi-active seat suspensions, the energy consumption and cost of active suspensions are high.

Electromagnetic seat suspension, which can transform electrical energy into mechanical energy to attenuate vibration and provide an ideal active control force, is a typical active suspension. Additionally, electromagnetic suspensions also can work as a generator to transform vibration energy into electrical energy. The energy can be consumed by electrical components, which can achieve vibration isolation. Additionally, the energy also can be harvested by storage components, such as batteries and supercapacitors. Therefore, semi-active electromagnetic suspensions have drawn increasing attention [14, 20–22]. Semi-active electromagnetic seat suspensions can achieve vibration suppression performance by varying damping [23], stiffness [24], and inertance [25] ways. In addition, some novel seat suspensions, which combine variable damping, variable stiffness, and variable inertance characteristics, achieve better vibration isolation performance than traditional dampers [14, 26, 27].

The energy dissipated by vehicle suspensions is very considerable, which accounts for about 3–12% of the total vehicle fuel consumption [20]. Therefore, it is necessary to study the energy recovery capacity of electromagnetic suspensions. The energy-harvesting characteristic of electromagnetic suspensions has been researched by many scholars and engineers, but few studies combine energy saving and vibration control. To cut this edge, a novel H-bridge-based electromagnetic damper (EMD) is designed [28]. To maximize the energy harvesting efficiency, an energy harvesting model and an optimal circuit structure are proposed for an electromagnetic inertial mass damper (EIMD) [22].

A continuously controllable EMD system is proposed, and the vibration control capacity is validated [23]. The damping of the EMD system can be controlled by changing the pulse-width modulation (PWM) duty cycle exerted on the MOSFET. Based on the EMD system, another variable damping strategy is developed by controlling the circuit resistance of the EMD system [3]. The EMD system has excellent vibration isolation performance, and the energy consumption of the EMD system can be neglected, which shows good application potential.

Although the above research has proved the vibration control performance of the EMD system, the robust controller [23] and sliding controller [3] are designed based on the assumption that absolute signals in the suspension system can be measured. Nevertheless, absolute signals cannot be measured easily because of the uneven road. In addition, the suspension system's disturbance has a serious effect on vibration control, so it is necessary to compensate for the disturbance of the seat suspension system [29].

To overcome the above issues, this paper proposes a robust controller based on state estimation and disturbance compensation and adopts the EMD seat suspension system with outstanding vibration isolation performance and energy-saving potential. The main contributions of this paper are highlighted below:

(a) Disturbance force of the EMD seat suspension system is compensated. A simple bench test is established to measure disturbance force–displacement data of the seat suspension. The Bouc–Wen model has been selected to represent the disturbance force.
(b) A robust H_∞ controller based on state observer and disturbance compensation is proposed. Since some state variables cannot be measured easily, a state observer is designed to estimate state variables that cannot be measured easily.
(c) Experimental studies of the robust controller based on disturbance compensation and state estimation are conducted on a six-DOF motion platform.

This paper is organized as follows: the next section introduces the seat suspension model, EMD model, and the system's disturbance model; the following section designs the robust controller based on disturbance compensation and state observer; the next section discusses the experimental platform and the experimental results; Conclusions are discussed in the last section.

Modelling of Seat Suspension System Equipped with the EMD System

The Variable Damping Seat Suspension Model

The vertical vibration influences the ride comfort most and generally has the highest magnitude in the seat suspension.

Thus, considering the system cost and effectiveness, most researchers study the vertical motion of the seat suspension without considering other directions' motions.

Figure 1a shows the schematic diagram of a seat with the EMD suspension system. The seat system consists of a spring, a seat with a scissor structure, and an EMD system. To simplify the controller design process, some simplified suspension models are adopted in previous studies [13, 16]. Seat suspension model supplemented with a human body model has been studied in previous studies, such as the four-DOF human body model [16]. However, most researches adopted a single DOF human model during the design process of controllers to simplify the problem [16]. A two-DOF suspension model is employed in this research and can be seen in Fig. 1b, where z_b, z_s and z_v are absolute displacements of driver body, suspension upper platform and vehicle cabin floor; m_b and m_s are the equivalent masses of the human body and seat suspension; k_b and k_s are the equivalent stiffness of human body and seat suspension; c_b and c_s are the equivalent damping coefficient of human body and seat suspension; f_r and u are equivalent disturbance force and output force of the EMD system, respectively.

The mathematical model of the seat suspension system equipped with the EMD system can be described as:

$$m_b \ddot{z}_b = -k_b(z_b - z_s) - c_b(\dot{z}_b - \dot{z}_s) \tag{1}$$

$$m_s \ddot{z}_s = k_b(z_b - z_s) + c_b(\dot{z}_b - \dot{z}_s) - k_s(z_s - z_v) - c_s(\dot{z}_s - \dot{z}_v) - f_r + u \tag{2}$$

The system state variables are selected as $x_1 = z_s - z_v, x_2 = \dot{z}_s, x_3 = z_b - z_s, x_4 = \dot{z}_b$. Then, the system state-space equation can be obtained based on Eqs. (1) and (2),

$$\dot{x} = Ax + B_1 w + B_2(u - f_r) \tag{3}$$

where $\dot{x} = \begin{bmatrix} x_1 & x_2 & x_3 & x_4 \end{bmatrix}^T$, $w = \dot{z}_v$,

$$A = \begin{bmatrix} 0 & 1 & 0 & 0 \\ -\frac{k_s}{m_s} & -\frac{c_b+c_s}{m_s} & \frac{k_b}{m_s} & \frac{c_b}{m_s} \\ 0 & -1 & 0 & 1 \\ 0 & \frac{c_b}{m_b} & -\frac{k_b}{m_b} & -\frac{c_b}{m_b} \end{bmatrix}, B_1 = \begin{bmatrix} -1 \\ \frac{c_s}{m_s} \\ 0 \\ 0 \end{bmatrix}, B_2 = \begin{bmatrix} 0 \\ \frac{1}{m_s} \\ 0 \\ 0 \end{bmatrix}.$$

In the practical situation, the vertical human body acceleration $\ddot{z}_b$, seat suspension upper platform acceleration $\ddot{z}_s$ and suspension relative displacement $z_s - z_v$ can be measured easily. Therefore, the control output can be written as,

$$Y = [\ddot{z}_b \ddot{z}_s z_s - z_v]^T = C_1 x + D_1 w + D_2(u - f_r) \tag{4}$$

where $C_1 = \begin{bmatrix} 0 & \frac{c_b}{m_b} & -\frac{k_b}{m_b} & -\frac{c_b}{m_b} \\ -\frac{k_s}{m_s} & -\frac{c_b+c_s}{m_s} & \frac{k_b}{m_s} & \frac{c_b}{m_s} \\ 1 & 0 & 0 & 0 \end{bmatrix}$, $D_1 = \begin{bmatrix} 0 \\ \frac{c_s}{m_s} \\ 0 \end{bmatrix}$,

$$D_2 = \begin{bmatrix} 0 \\ \frac{1}{m_s} \\ 0 \end{bmatrix}.$$

The main research objective of the seat suspension controller is to improve ride comfort, and the human body acceleration is regarded as a ride comfort index. In addition, many operation devices, such as the accelerator pedal, brake pedal, and transmission lever, are fixed on the cabin floor. Therefore, an excessive seat suspension deflection may cause handling problems. Additionally, the seat suspension with a large deflection may hit the stop block, which will deteriorate the ride comfort. Therefore, seat suspension acceleration $\ddot{z}_b$ and seat suspension deflection $z_s - z_v$ are defined as two main performance criteria. Thus,
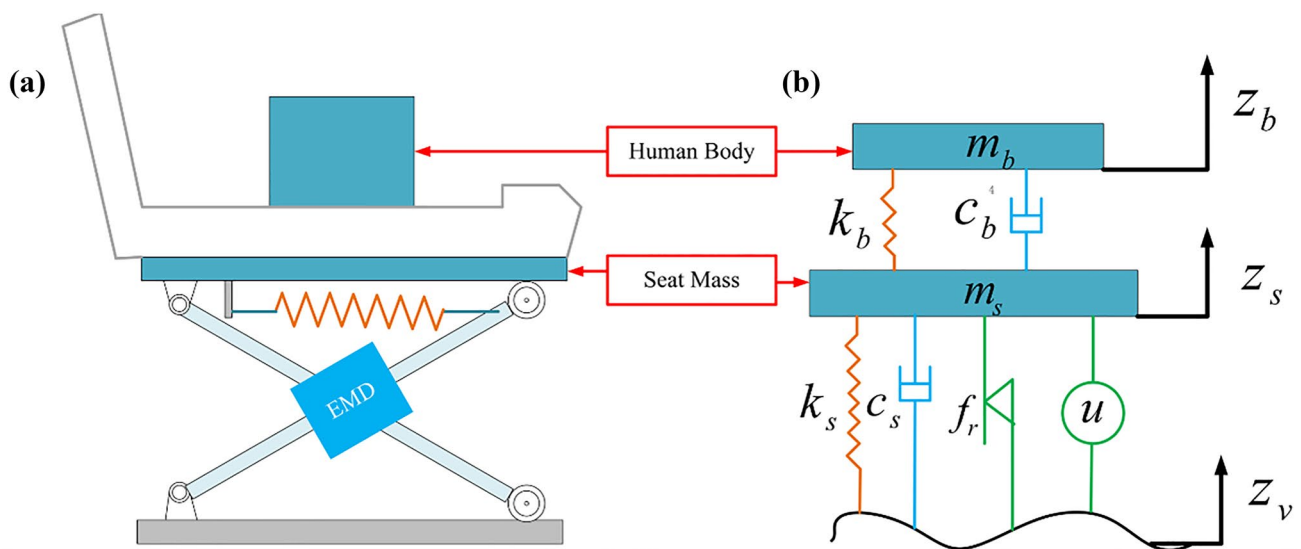

Fig. 1 Seat suspension system **a** schematic diagram of a seat with suspension; **b** seat suspension mathematical model

the controllable output is defined as $Z = [\ddot{z}_s z_s - z_v]^T$ and can be obtained as,

$$Z = [\ddot{z}_b z_s - z_v]^T = \delta Cx \tag{5}$$

where $\delta = \begin{bmatrix} \delta_1 & 0 \\ 0 & \delta_2 \end{bmatrix}$, $C = \begin{bmatrix} 0 & \frac{c_b}{m_b} & -\frac{k_b}{m_b} & -\frac{c_b}{m_b} \\ 1 & 0 & 0 & 0 \end{bmatrix}$; δ is the weighting matrix, which determines seat suspension ride comfort and handling stability performance. δ_1 and δ_2 are the weighting parameters, which are identified by trial and error. A larger δ_1 usually was selected compared with δ_2 because ride comfort is the primary control objective of the designed controller.

Modelling of the EMD System

The prototype and equivalent circuit frame diagram of the EMD system can be seen in Figs. 2 and 3. As can be seen from Fig. 2 the EMD system consists of a permanent magnet synchronous motor (PMSM), a three-phase rectifier, an external resistor, and an N-channel metal–oxide–semiconductor field-effect transistor (MOSFET). Figure 3 shows the circuit diagram in detail, where e, L_i, R_i are the generated voltage, inner inductance, and inner resistance of the

EMD system, respectively; R_e is the external resistance of the EMD system. The MOSFET is connected with R_e in parallel. The functionality of the circuit is to provide controllable varying damping force by changing the equivalent circuit current. The controller sends PWM duty cycle signals to the MOSFET, and the equivalent resistance of the whole circuit can be changed with the change of the PWM signals. Therefore, the equivalent circuit current is changed according to the change of circuit equivalent resistance.

When the seat suspension moves, the PMSM will generate a voltage, which is proportional to the circuit current [30, 31]. The PMSM will generate an output torque proportional to the circuit current. The output torque will be converted into vertical force through the scissors structure of the seat suspension. Therefore, the damping force can be controlled by controlling circuit current, which can be realized by changing circuit equivalent resistance. Therefore, the equivalent circuit resistance of the EMD system can be controlled by exerting different PWM duty cycles of the MOSFET switch.

The EMD system is installed on a seat suspension, and its structures can be seen in Fig. 4. The reducer shell is fixed on the outer rod of the scissors structure, while the rotating shaft of the reducer is fixed on the inner rod of the scissors
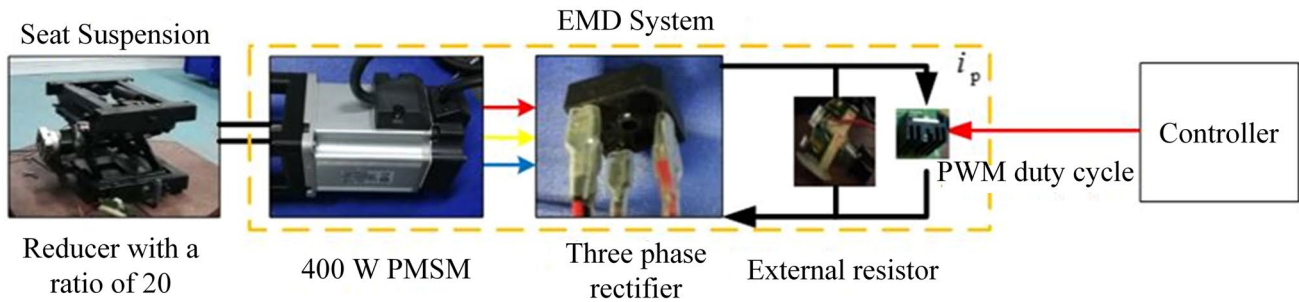

Fig. 2 EMD seat suspension prototype
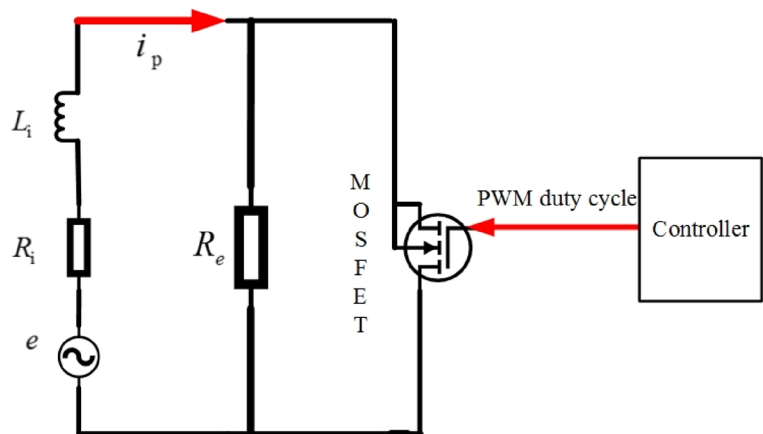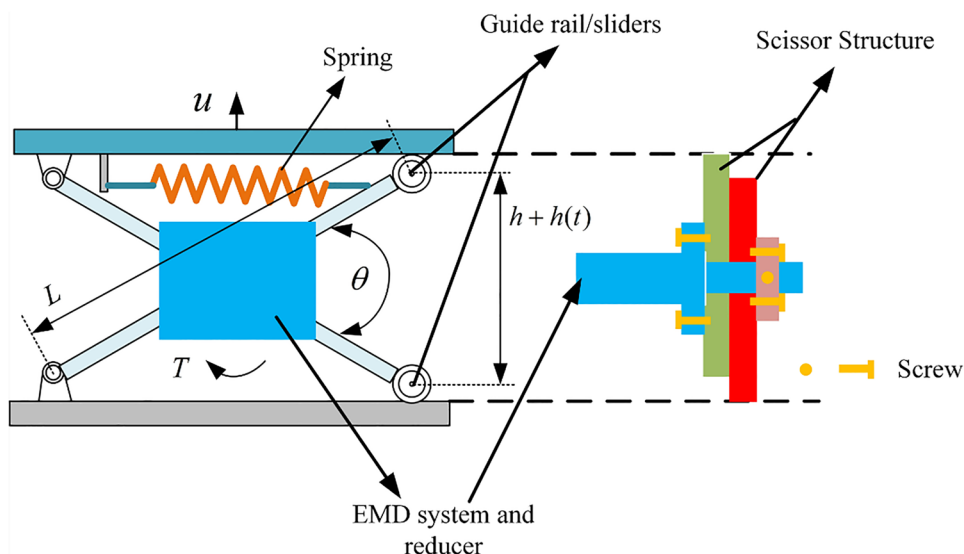
Fig. 3 Control circuit diagram

Fig. 4 The kinetic model of the seat suspension

structure. When the vehicle moves vertically, the sliders of the seat suspension slide in the guide rail, and the two rods of the scissors structure drive the shell and the shaft of the motor to rotate respectively. Therefore, the scissors structure can output a changing angle θ. The vertical movement of the seat suspension transformed into the rotary movement of the EMD system in this way. In this way, the rotary output torque T is transformed into the vertical force u to the seat suspension.

When the rotor of the PMSM is rotating, a voltage proportional to rotational speed is generated in the circuit. PMSM will output a real-time changing torque proportional to circuit current because of the changing resistance, and the torque of the PMSM will be amplified by the reducer. The amplified torque is transmitted to the scissors structure of the seat suspension by the motion transmission path. Then the sliders slide into the guide rail, and the torque is transformed into vertical force and acts on the seat suspension.

The output force of the EMD system can be obtained by the relationship between the seat suspension and the EMD system [23],

$$u = \frac{4r_g^2 k_i^2}{\left(L^2 - (h + h(t))^2\right)\left(R_i + (1 - D)R_e\right)}\dot{h}(t) \quad (6)$$

where r_g is the gear ratio of the reducer; k_i is the torque constant of the PMSM; L is the length of the seat suspension rod; h_0 is the initial height of the seat suspension; h is the relative displacement of the seat suspension; $\dot{h}$ is the relative velocity of the seat suspension; R_i is the internal resistance; R_e is the external resistance; D is the PWM duty cycle.

The Equivalent Disturbance Force Model

In the seat suspension system equipped with the EMD system, there are two disturbances. One is caused by the road roughness, which is the cabin floor acceleration $\ddot{z}_v$. In the robust controller design process, the cabin floor acceleration $\ddot{z}_v$ is defined as system disturbance. Another one is friction and equivalent inertial force. The friction force comes from the mechanical system, and the equivalent inertial force is caused by the rotor of the permanent magnet synchronous motor (PMSM) and the reducer. The friction and the inertial force have an unneglectable impact on the seat suspension dynamics. Therefore, the disturbance force containing the friction and equivalent inertial force is estimated for enhancing controlling performance.
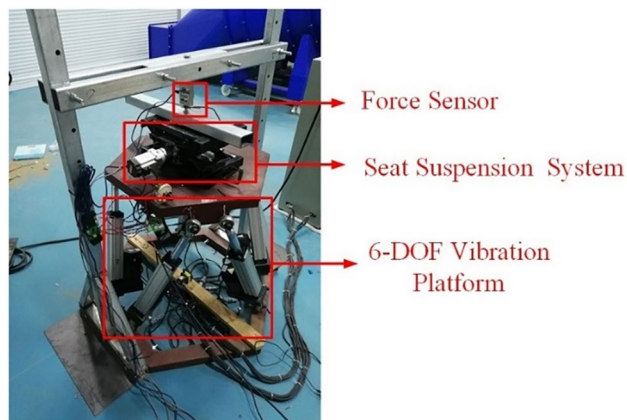

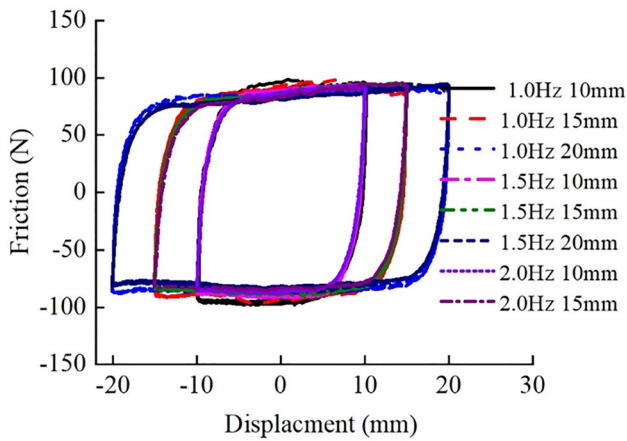**Fig. 5** The experimental setup of test bench for seat suspension disturbance force

Fig. 6 Disturbance force–displacement relationship

To compensate for the disturbance force, a 6-DOF vibration platform and a force sensor are applied to measure the force–displacement relationship of the seat suspension (the damper of the seat suspension is removed). The experimental bench is shown in Fig. 5 and the displacement excitation data can be seen in Fig. 6.

The six-DOF vibration platform is fixedly connected with the seat suspension system to provide the vertical displacement excitation and the real-time suspension force is measured by the force sensor. Since the damper is removed, the force obtained from the experiments includes disturbance force and stiffness force. As the suspension stiffness is already known, the disturbance-displacement responses can be obtained in Fig. 6. Since the disturbance force–displacement response is known, the disturbance force–velocity can be obtained by deriving the displacement.

Compared with the equivalent inertial force, the friction force has a greater influence on suspension vibration control. The friction forces with the excitation frequencies of 1 Hz, 1.5 Hz, and 2 Hz are overlapping. When the seat suspension deflection directions are inversed, there is an apparent hysteresis phenomenon in the change of friction force.

Therefore, a hysteresis model (Bouc–Wen model) is chosen to describe the disturbance because the model widely used in the MR model to describe the hysteresis characteristics [32]. The Bouc-Wen model is given as:

$$\begin{cases} \widehat{f}_r = \alpha z_d \\ \dot{z}_d = -\gamma_d |v_s| z_d |z_d| - \beta_d v_s |z_d|^2 + A_d (\dot{z}_s - \dot{z}_v) \end{cases} \quad (7)$$

where $\dot{z}_s - \dot{z}_v$ is the relative velocity of the seat suspension; z_d is the intermediate variable; α, γ_d, β_d and A_d are the parameters to be identified.

Robust Controller Design

Design of State Observer

In the practical scene, human body deflection, human body, and seat suspension's absolute velocity cannot be measured easily because sensors cannot be installed easily. Therefore, only seat suspension relative displacement x_1 is easy to be measured in all state variables.

A state observer is designed to solve the problem and the estimated control output can be defined based on Eq. (4),

$$\widehat{Y} = C_1 \hat{x} + D_2 \left(u - \widehat{f}_r \right), \quad (8)$$

where $\widehat{f}_r$ is the estimated disturbance force.

The estimation error is,

$$e = x - \hat{x}. \quad (9)$$

Therefore, the state observer can be obtained by,

$$\dot{\hat{x}} = A\hat{x} + B_2 \left(u - \widehat{f}_r \right) + L \left(Y - \widehat{Y} \right), \quad (10)$$

where $\hat{x}$ is the estimated state variables, L is the state observer gain. Therefore, state variables can be estimated by damping force, disturbance force and control output.

By differentiating Eq. (9), the derivative of the estimation error can be obtained by substituting Eqs. (3), (4), (8) and (10) into Eq. (9):

$$\dot{e} = \dot{x} - \dot{\hat{x}} = (A - LC_1)e + (B_1 - LD_1)w + (LD_2 - B_2)e_f. \quad (11)$$

Robust H_∞ controller design

The robust H_∞ controller is designed as,

$$u = K\hat{x} + \widehat{f}_r \quad (12)$$

where K is the feedback gain to be solved.

The state equation can be rearranged by substituting Eqs. (9), (12) into Eq. (3),

$$\dot{x} = (A + B_2 K)x + B_1 w - B_2 Ke - B_2 e_f. \quad (13)$$

A new state-space equation is obtained by augmenting matrix,

$$\dot{\bar{x}} = A_h \bar{x} + B_h d, \quad (14)$$

where $\bar{x} = \begin{bmatrix} x \\ e \end{bmatrix}$; $A_h = \begin{bmatrix} A + B_2K & -B_2K \\ 0 & A - LC_1 \end{bmatrix}$;
$B_h = \begin{bmatrix} B_1 & -B_2 \\ B_1 - LD_1 & LD_2 - B_2 \end{bmatrix}$; $d = \begin{bmatrix} w \\ e_f \end{bmatrix}$.

Then Eq. (5) can be rewritten as

$$Z = C_h\bar{x} \tag{15}$$

where $C_h = \begin{bmatrix} C & 0 \end{bmatrix}$.

To satisfy system's H_∞ performance, the designed controller should be asymptotically stable when $\tilde{w} \equiv 0$. The H_∞ norm is chosen as the control performance measure. The L_2 gain of the system (14) and (15) is defined as,

$$\left\| T_{zd} \right\|_\infty = \sup \frac{\|Z\|_2}{\|d\|_2}, \tag{16}$$

where $\|Z\|_2 = \int_0^\infty Z_{(t)}^T Z_{(t)} dt$; $\|d\|_2 = \int_0^\infty d_{(t)}^T d_{(t)} dt$.

The Lyapunov function of (14) is,

$$V = \bar{x}^T P\bar{x} \tag{17}$$

where $P = \begin{bmatrix} P_1 & 0 \\ 0 & P_2 \end{bmatrix}$ is a positive matrix, $P = P^T$, and P_1 and P_2 are both positive definite matrices.

$$\Omega = \begin{bmatrix} A_h^T P + PA_h & PB_h & C_h^T \\ B_h^T P & -\gamma^2 I & 0 \\ C_h & 0 & -1 \end{bmatrix} < 0. \tag{21}$$

Equation (21) is post- and pre-multiplied by diag (P_1^{-1}, I, I, I, I) and its transposition matrix, respectively. Then we define $P_1^{-1} = Q$, $KQ = Y$, $P_2L = G$, where P_2 is a constant matrix. The controller gain and observer gain can be obtained by solving the following linear matrix inequality (LMI),

$$\Omega = \begin{bmatrix} AQ + B_2Y + * & -B_2K & B_1 & -B_2 & QC^T \\ * & P_2A - GC_1 + * & P_2B_1 - GD_1 & GD_2 - P_2B_2 & 0 \\ * & * & -\gamma^2 I & 0 & 0 \\ * & * & * & -\gamma^2 I & 0 \\ * & * & * & * & -I \end{bmatrix} < 0 \tag{22}$$

By differentiating Eq. (17), and the equation can be obtained,

$$\dot{V} = \dot{\bar{x}}^T P\bar{x} + \bar{x}^T P\dot{\bar{x}}. \tag{18}$$

Adding $Z^T Z - \gamma^2 d^T d$ to the two sides of Eq. (18) can obtain,

$$\dot{V} + Z^T Z - \gamma^2 d^T d = \begin{bmatrix} \bar{x}^T & d^T \end{bmatrix} \begin{bmatrix} A_h^T P + PA_h + C_h^T C_h & PB_h \\ B_h^T P & -\gamma^2 I \end{bmatrix} \begin{bmatrix} \bar{x} \\ d \end{bmatrix} \tag{19}$$

where γ is the H_∞ performance criteria.

If we define

$$\Omega = \begin{bmatrix} A_h^T P + PA_h + C_h^T C_h & PB_h \\ B_h^T P & -\gamma^2 I \end{bmatrix} < 0, \tag{20}$$

then $\dot{V} + Z^T Z - \gamma^2 d^T d < 0$.

By the Schur complement, $\Omega < 0$ is equivalent to

Table 1 Parameters of seat suspension system and controller

Parameters	Symbols	Values	Units
Human body mass	m_b	80	kg
Seat suspension mass	m_s	15	kg
Human body stiffness	k_b	90,000	N/m
Human body damping	c_b	2000	Ns/m
Seat suspension stiffness	k_s	7850	N/m
Seat suspension damping	c_s	10	Ns/m
Weighting parameters	δ_1	0.04	–
	δ_2	0.01	–
Controller performance index	γ	1	–
–	P_2	10	–

where $Q = Q^T$, $Q > 0$. After solving the Eq. (22) for matrices Q, Y and G, the controller gain and the observer gain are obtained as $K = YQ^{-1}$, $L = P_2^{-1}G$.

Case Study

To validate the effectiveness of the proposed control algorithm, a specific case is studied. The seat suspension system and controller parameters are listed in Table 1. The parameters of the seat system are measured in a laboratory, while the human body stiffness and damping coefficients are from reference [33]. It is worth mentioning that although there is no damper in the suspension system, a small damping coefficient is selected since the system still exists a linear damping part. The control gain can be obtained as $K = \begin{bmatrix} 7828.3 & 1711.1 & -68153 & -1726.2 \end{bmatrix}$, and the state observer gain is $L = \begin{bmatrix} -7.9229 & -1.4855 & -244.8603 \\ 0.0012 & 1 & 0 \\ 0 & 0 & -0.0011 \\ 0.9988 & 0 & 0 \end{bmatrix}$.
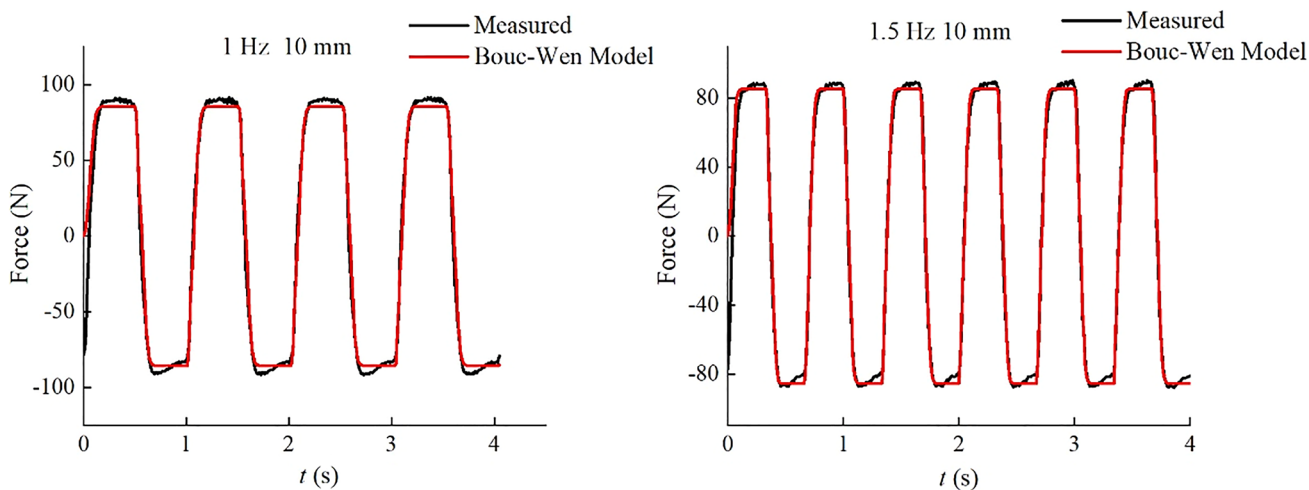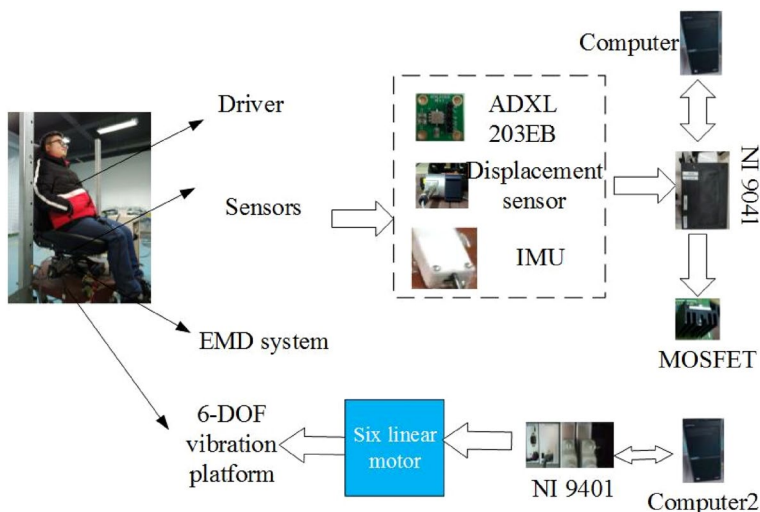
Fig. 7 Disturbance force simulation

Fig. 8 Test rig setup

The Simulink design optimization toolbox is used to identify parameters of the Bouc-Wen model and these parameters can be identified as $A_d = -517{,}920$, $\alpha = -110.22$, $\beta_d = 1{,}724{,}900$, $\gamma_d = 2{,}586{,}600$. The simulated disturbance force is compared with the measured disturbance force in Fig. 7. Figure 7 shows that the Bouc-Wen model is highly consistent with experimental data, which validates the effectiveness of the disturbance compensation method.

Experimental Validation

Experimental Setup

The seat suspension system equipped with the EMD system is tested on a 6-DOF vibration platform, and the test rig is shown in Fig. 8. The 6-DOF vibration platform is applied to generate vertical vibration excitation. A c-RIO 9076 and three NI 9401 are used to control the motion of the 6-DOF vibration platform.

A displacement sensor is used to measure seat suspension deflection. Two acceleration sensors (ADXL 203EB) are used to measure acceleration data of the seat suspension upper platform and six-DOF upper platform, respectively. In addition, an inertial measurement unit (IMU) is applied to measure the human body's acceleration since the human body has coupled motions. An NI 9041 can send PWM duty cycle signals to control the EMD system. A current sensor is used to measure the current of the circuit diagram. The measurement and control frequency is set as 500 Hz. Measurement data from these sensors are required by this controller and then the desired PWM duty cycles are sent out to the EMD system.

Table 2 Sinusoidal excitations signals

Frequency, Hz	1	1.2	1.4	1.6	1.8	2	2.5	3
Amplitude, mm	30	25	23	17	15	13	10	7

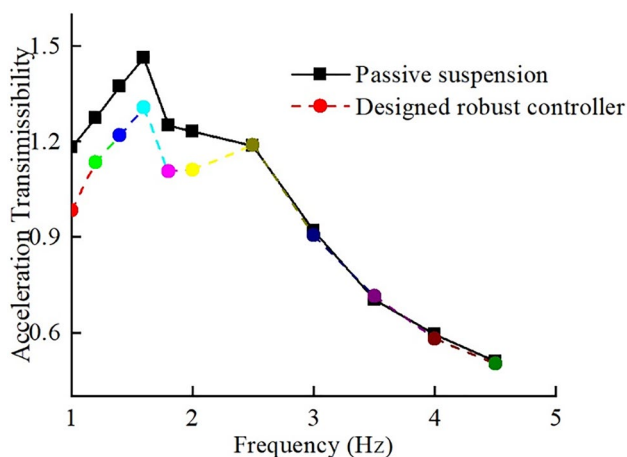**Fig. 9** Acceleration transmissibility

Fig. 10 Human body acceleration response under bump excitation

To validate the effectiveness of the controller, a well-tuned commercial suspension is selected to compare with the semi-active seat suspension. Besides that, three different types of experiments (sinusoidal vibration, bump excitation, and random excitation) were carried out.

Experimental Results

Sinusoidal Excitation

To systematically research the EMD seat suspension's vibration suppression performance under different frequencies, sinusoidal excitations are applied. Acceleration transmissibility is used to evaluate the controller's performance, and Table 2 shows sinusoidal excitations' frequency and amplitude.

The acceleration transmissibility of the system can be obtained,

$$T_{bv} = \frac{\text{RMS}(\ddot{z}_b)}{\text{RMS}(\ddot{z}_v)} \tag{23}$$

where $\text{RMS}(\ddot{z}_b)$ is the root mean square (RMS) value of human body acceleration; $\text{RMS}(\ddot{z}_v)$ is the RMS value of the 6-DOF upper platform; $\text{RMS}(a) = \sqrt{\frac{1}{N}\sum_{i=1}^{N} a_i^2}$.

The comparison of suspension acceleration transmissibility is shown in Fig. 9. It can be seen that the resonance frequency of the seat suspension is around 1.6 Hz and the designed controller can reduce resonance vibration effectively. In addition, the robust controller can
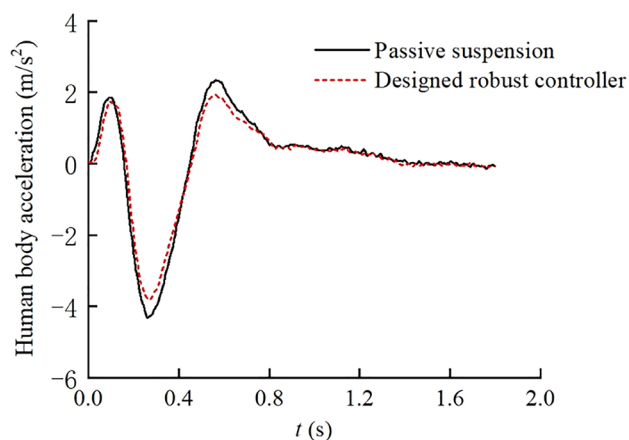
isolate vibration effectively in the lower frequency band (1–2.5 Hz), while the robust controller can keep a similar passivity performance with the passive suspension in the higher frequency band ($f > 2.5$ Hz).

It is worth mentioning that the high-frequency excitation of the uneven road will be filtered by the vehicle suspension in practice. Therefore, the designed controller is useful in practical scenarios because it can reduce vibration effectively in low frequency and keep passivity in high frequency.

Bump Excitation

Bump excitation usually is used to evaluate the suspension system's transient response characteristics, and the excitation is given in reference [13]. Relevant excitation can be obtained by exerting the bump excitation on a seven-DOF vehicle model. The response of the 7-DOF vehicle model is used as the input of the seat suspension. The Bump excitation is given as follows

$$Z_r(t) = \begin{cases} \frac{a}{2}\left(1 - \cos\left(\frac{2\pi v_0}{l}t\right)\right), & 0 \leq t \leq \frac{l}{v_0} \\ 0, & t > \frac{l}{v_0} \end{cases} \tag{24}$$

where $a = 0.04$ m, $l = 0.4$ m are the height and length of the Bump excitation, and the forward velocity $v_0 = 9.7$ m/s.

Figure 10 demonstrates that the robust controller can improve the seat suspension system's transient response
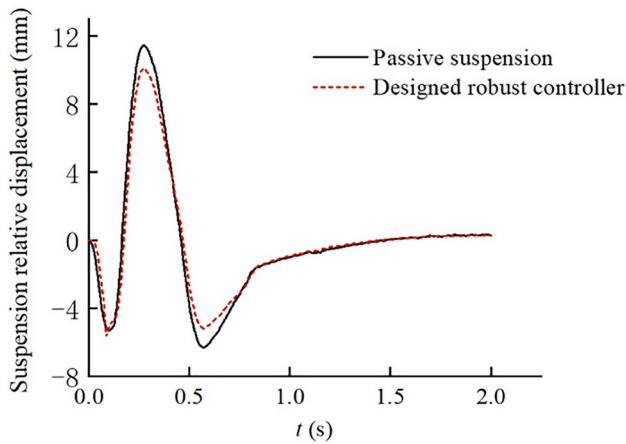
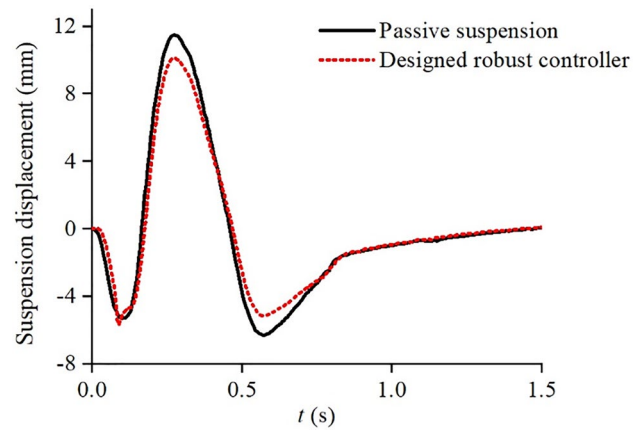**Fig. 11** Seat suspension relative displacement response under bump excitation

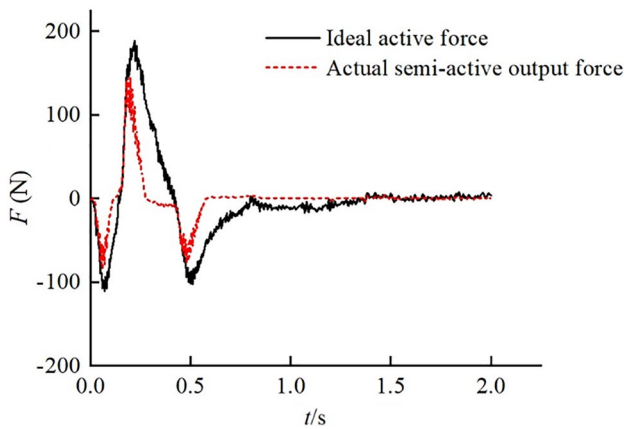**Fig. 13** The performance of state observer

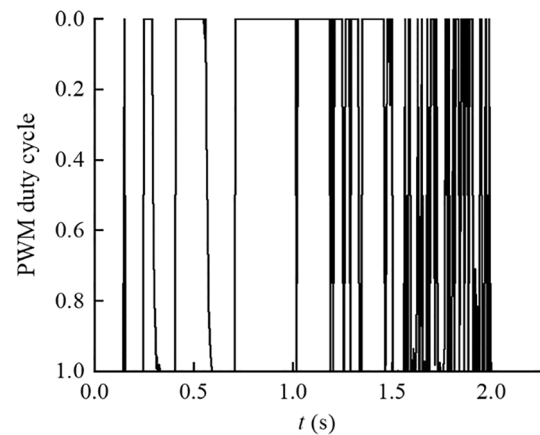**Fig. 12** The actual output force and ideal active force

Fig. 14 PWM duty cycle

performance effectively. The first peak acceleration values of the passive suspension and EMD seat suspension are 1.858 m/s² and 1.706 m/s², and the second peak acceleration values are 2.3505 m/s² and 1.5863 m/s², respectively.

This means that the EMD seat suspension's peak acceleration values have declined by 8.18% and 32.5% compared with the passive suspension. In addition, the robust controller can reduce shock quickly compared with the passive one.

Figure 11 shows that EMD seat suspension's handling performance is improved, which means that the relative displacement has declined compared with the passive suspension. The EMD seat suspension and passive suspension's relative displacement peak values are 11.451 mm and 8.975 mm, separately. This means that the relative displacement peak value of the EMD seat suspension has declined by nearly 21.6% compared with the passive suspension.

Figure 12 demonstrates the comparison between the active force obtained by the robust controller and the actual

output force, and the semi-active force can track the active force well. Based on the above analysis, only the state variable x_1 can be easily measured in practice. Therefore, the estimated state variable $\hat{x_1}$ and practical state variable x_1 are compared in Fig. 13, and the error between $\hat{x_1}$ and x_1 is very little. The effectiveness of the designed state observer is validated. In addition, the real-time duty cycle calculated by the robust controller is shown in Fig. 14.

Random Excitation

The random excitation is closer to the actual road excitation, the random excitation is selected as the seat suspension's input,

$$\dot{z}_r(t) + \rho V Z_r(t) = V W_n \tag{25}$$

where W_n is the intensity $2\sigma^2 \rho V$ of the white noise, σ^2 is the covariance of road irregularity; V is the vehicle forward
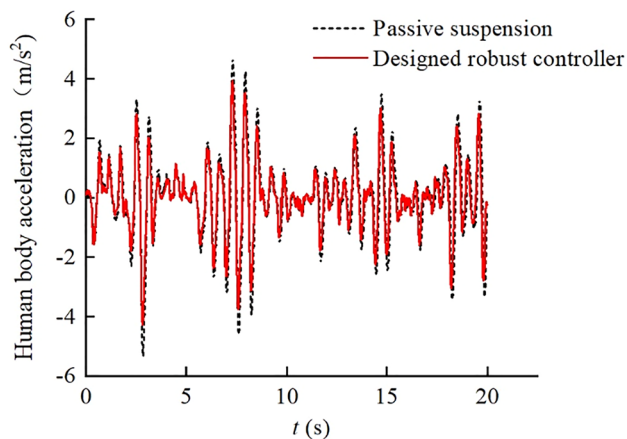
Fig. 15 Human body acceleration under random excitation
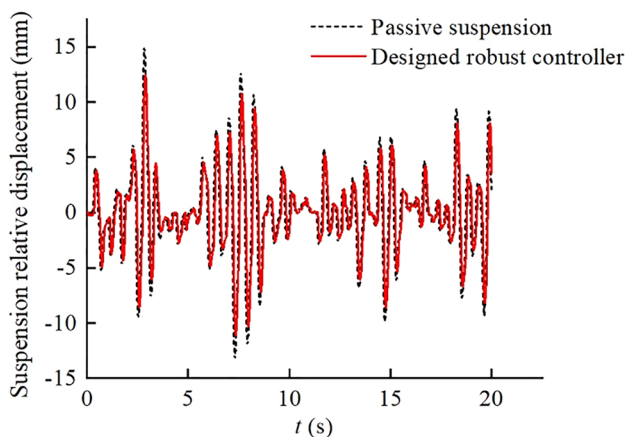

Fig. 16 Seat suspension relative displacement response under random excitation

velocity; ρ is the road roughness parameters. $\rho = 0.45$ m^{-1}, $\sigma^2 = 300$ mm^2, $v = 20$ ms^{-1} are chosen in this paper. Similarly, the 7-DOF vehicle model is used to generate random responses and the response signals are used as seat suspension random input.

The acceleration response and seat suspension relative displacement are shown in Figs. 15 and 16, respectively. The seat suspension based on the robust controller achieves better vibration isolation and handling performance compared with the passive suspension under random excitation conditions.

To evaluate the controller's performance under random excitation quantitatively, ISO 2631-1 is applied to evaluate the two kinds of seat suspensions. The RMS, frequency-weighed root mean square (FW-RMS), and fourth power vibration dose value (VDV) are calculated as follows,
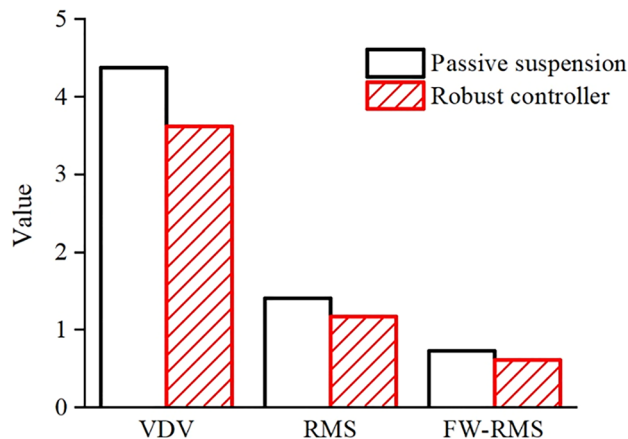

Fig. 17 The comparison of the VDV, RMS and FW-RMS

$$\text{RMS} = \sqrt{\frac{1}{N} \sum_{i=1}^{N} a_i^2}, \tag{26}$$

$$a_{\text{FW-RMS}} = \left[\frac{1}{T} \int_0^T a_w^2(t)\mathrm{d}t \right]^{1/2} \tag{27}$$

$$\text{VDV} = \left[\frac{1}{T} \int_0^T a_w^4(t)\mathrm{d}t \right]^{1/4}, \tag{28}$$

where a_w is the frequency-weighted acceleration.

It can be seen from Fig. 17 that the VDV, RMS, and FW-RMS values of the EMD seat suspension are 4.3706 m/s^2, 1.4098 m/s^2, and 0.7266 m/s^2, while the corresponding values of the passive suspension are 3.6145 m/s^2, 1.1763 m/s^2, and 0.6142 m/s^2, respectively. This means that the VDV, RMS and FW-RMS values of the EMD seat suspension have dropped 17.30%, 16.56%, and 11.24% compared with the passive one, respectively.

In addition, the RMS values of relative displacement are calculated to evaluate seat suspension's handling performance quantitatively. Figure 18 illustrates the seat suspension relative displacement RMS values. The relative displacement RMS values are 3.5049 mm and 4.0328 mm for the EMD seat suspension and the passive suspension, which means that the EMD seat suspension's handling stability has increased by 13.09% than the passive one.

To further investigate the robust controller's frequency characteristics, the acceleration power spectral density (APSD) is compared in Fig. 19. Figure 19 shows that the passive suspension and the EMD seat suspension both
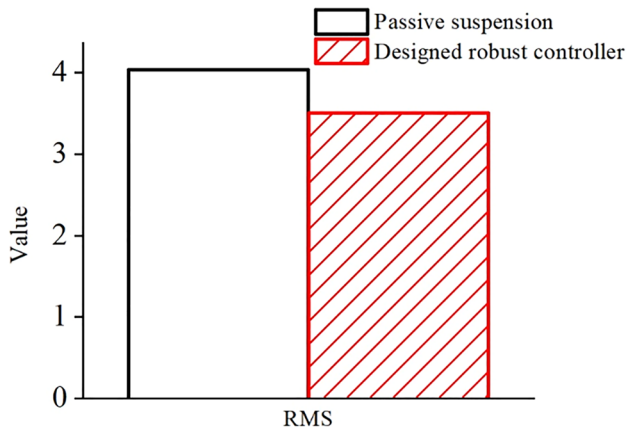
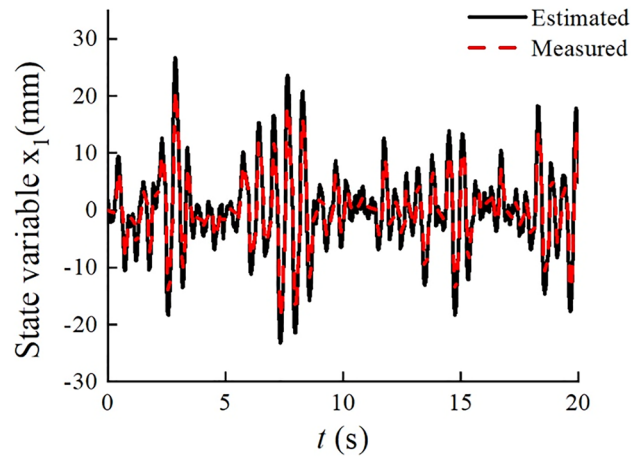**Fig. 18** The relative displacement RMS values

Fig. 21 State observer performance
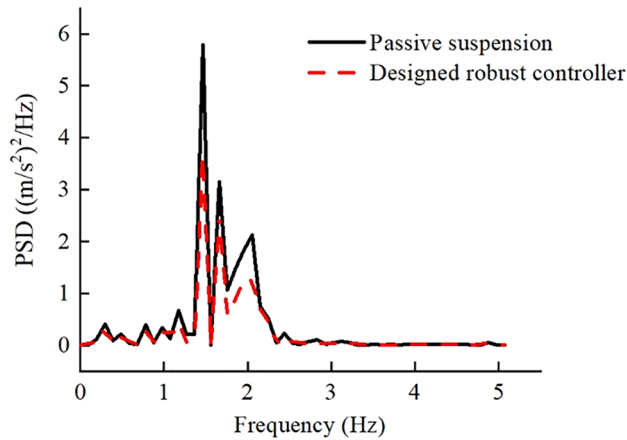
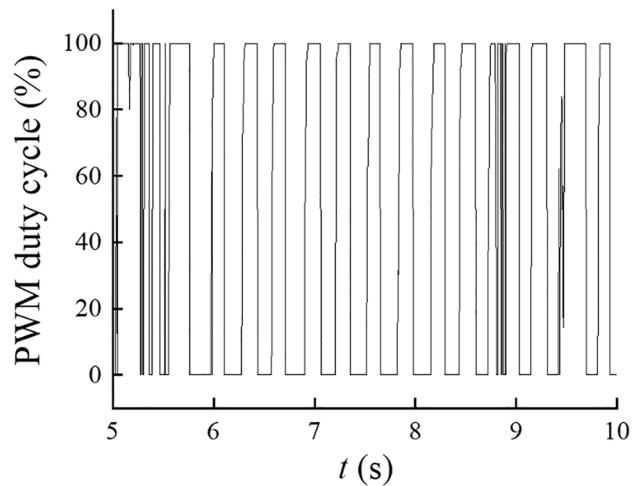

Fig. 19 PSD of human body acceleration

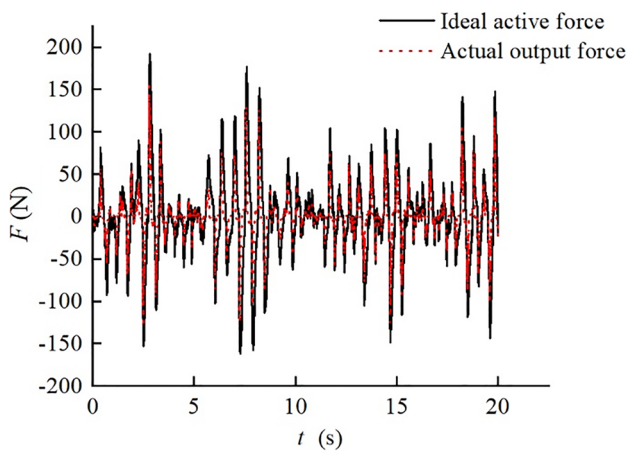**Fig. 22** PWM duty cycle

Fig. 20 Response of actual output force under random excitation

have a peak value of around 1.46 Hz. The robust controller can suppress the vibration to a very low magnitude in a wide frequency range (0.1–4 Hz). The APSD peak values of the EMD seat suspension and the passive suspension are 5.8097 $(m/s^2)^2$/Hz and 3.611 $(m/s^2)^2$/Hz, which means that the APSD peak value of the EMD seat suspension has decreased by 37.84% compared with the passive one.

The performance of actual output force, state observer, and output PWM duty cycle is shown in Figs. 20, 21 and 22. The EMD system can achieve the requirement of ideal active force to a larger extent, and the state observer has good performance with little estimation error.

Conclusions

This paper proposes an applicable robust controller, which can compensate for the system disturbance and estimate state variables effectively. Compared with a well-tuned commercial passive suspension, the proposed controller has better overall performance. Conclusions are summarized as follows.

1. The state controller can be implemented with the human body acceleration, seat suspension acceleration, and the seat suspension relative displacement signals. Experimental results show that the proposed observer has excellent performance with an acceptable estimation error.

2. The seat suspension disturbance force, including friction force, and inertia force, is measured on a test bench. The Bouc-Wen model is selected to compare with actual disturbance, which shows high accuracy.

3. Experimental results show that the controller has great vibration isolation performance and handling performance than a passive suspension under three typical road excitations. The VDV, RMS and FW-RMS values of the designed controller decreased by 17.30%, 16.56%, and 11.24%, respectively.

Declarations

Conflict of interest The authors declare that they have no known competing financial interests or personal relationships that could have appeared to influence the work reported in this paper.

References

1. Zhang N, Smith WA, Jeyakumaran J (2010) Hydraulically interconnected vehicle suspension: background and modelling. Veh Syst Dyn 48(1):17–40. https://doi.org/10.1080/004231109032431 82

2. Zeng M, Tan B, Ding F, Zhang B, Zhou H, Chen Y (2019) An experimental investigation of resonance sources and vibration transmission for a pure electric bus. Proc Inst Mech Eng Part D J Automob Eng 234(4):950–962. https://doi.org/10.1177/09544 07019879258

3. Liu P, Xia X, Zhang N, Ning D, Zheng M (2019) Torque response characteristics of a controllable electromagnetic damper for seat suspension vibration control. Mech Syst Signal Process. https://doi.org/10.1016/j.ymssp.2019.07.019

4. Zheng M, Zhang B, Zhang J, Zhang N (2016) Physical parameter identification method based on modal analysis for two-axis on-road vehicles: theory and simulation. Chin J Mech Eng 29(4):756–764. https://doi.org/10.3901/cjme.2016.0108.004

5. Zheng M, Peng P, Zhang B, Zhang N, Wang L, Chen Y (2015) A new physical parameter identification method for two-axis on-road vehicles: simulation and experiment. Shock Vib 2015:1–9. https://doi.org/10.1155/2015/191050

6. Du H, Lam J, Cheung KC, Li W, Zhang N (2013) Direct voltage control of magnetorheological damper for vehicle suspensions. Smart Mater Struct. https://doi.org/10.1088/0964-1726/22/10/105016

7. Sun S et al (2021) Experimental study of a variable stiffness seat suspension installed with a compact rotary MR damper. Front Mater. https://doi.org/10.3389/fmats.2021.594843

8. Sun SS, Ning DH, Yang J, Du H, Zhang SW, Li WH (2016) A seat suspension with a rotary magnetorheological damper for heavy duty vehicles. Smart Mater Struct. https://doi.org/10.1088/0964-1726/25/10/105032

9. Tu L et al (2020) A novel negative stiffness magnetic spring design for vehicle seat suspension system. Mechatronics. https://doi.org/10.1016/j.mechatronics.2020.102370

10. Liu Y-J, Zeng Q, Tong S, Chen CLP, Liu L (2019) Adaptive neural network control for active suspension systems with time-varying vertical displacement and speed constraints. IEEE Trans Ind Electron 66(12):9458–9466. https://doi.org/10.1109/tie.2019.2893847

11. Moradi M, Fekih A (2014) Adaptive PID-sliding-mode fault-tolerant control approach for vehicle suspension systems subject to actuator faults. IEEE Trans Veh Technol 63(3):1041–1054. https://doi.org/10.1109/tvt.2013.2282956

12. Tang X, Ning D, Du H, Li W, Wen W (2020) Takagi-Sugeno fuzzy model-based semi-active control for the seat suspension with an electrorheological damper. IEEE Access 8:98027–98037. https://doi.org/10.1109/access.2020.2995214

13. Ning D, Sun S, Zhang F, Du H, Li W, Zhang B (2017) Disturbance observer based Takagi-Sugeno fuzzy control for an active seat suspension. Mech Syst Signal Process 93:515–530. https://doi.org/10.1016/j.ymssp.2017.02.029

14. Tang X, Ning D, Du H, Li W, Gao Y, Wen W (2020) A Takagi-Sugeno fuzzy model-based control strategy for variable stiffness and variable damping suspension. IEEE Access 8:71628–71641. https://doi.org/10.1109/access.2020.2983998

15. Ning D, Sun S, Wei L, Zhang B, Du H, Li W (2017) Vibration reduction of seat suspension using observer based terminal sliding mode control with acceleration data fusion. Mechatronics 44:71–83. https://doi.org/10.1016/j.mechatronics.2017.04.012

16. Choi S-B, Han Y-M (2007) Vibration control of electrorheological seat suspension with human-body model using sliding mode control. J Sound Vib 303(1–2):391–404. https://doi.org/10.1016/j.jsv.2007.01.027

17. Li W, Du H, Ning D, Li W, Sun S, Wei J (2021) Event-triggered H∞ control for active seat suspension systems based on relaxed conditions for stability. Mech Syst Signal Process. https://doi.org/10.1016/j.ymssp.2020.107210

18. Zhang J, Zhang B, Zhang N, Wang C, Chen Y (2021) A novel robust event-triggered fault tolerant automatic steering control approach of autonomous land vehicles under in-vehicle network delay. Int J Robust Nonlinear Control 31(7):2436–2464. https://doi.org/10.1002/rnc.5393

19. Wu L, Gao Y, Liu J, Li H (2017) Event-triggered sliding mode control of stochastic systems via output feedback. Automatica 82:79–92. https://doi.org/10.1016/j.automatica.2017.04.032

20. Abdelkareem MAA et al (2018) Vibration energy harvesting in automotive suspension system: a detailed review. Appl Energy 229:672–699. https://doi.org/10.1016/j.apenergy.2018.08.030

21. Wang R, Ding R, Chen L (2016) Application of hybrid electromagnetic suspension in vibration energy regeneration and active

control. J Vib Control 24(1):223–233. https://doi.org/10.1177/1077546316637726

22. Zhu H, Li Y, Shen W, Zhu S (2019) Mechanical and energy-harvesting model for electromagnetic inertial mass dampers. Mech Syst Signal Process 120:203–220. https://doi.org/10.1016/j.ymssp.2018.10.023

23. Ning D, Du H, Sun S, Li W, Li W (2018) An energy saving variable damping seat suspension system with regeneration capability. IEEE Trans Ind Electron 65(10):8080–8091. https://doi.org/10.1109/tie.2018.2803756

24. Ning D et al (2020) An electromagnetic variable stiffness device for semiactive seat suspension vibration control. IEEE Trans Ind Electron 67(8):6773–6784. https://doi.org/10.1109/tie.2019.2936994

25. Ning D et al (2019) An electromagnetic variable inertance device for seat suspension vibration control. Mech Syst Signal Process. https://doi.org/10.1016/j.ymssp.2019.106259

26. Liu P, Ning D, Luo L, Zhang N, Du H (2021) An electromagnetic variable inertance and damping seat suspension with controllable circuits. IEEE Trans Ind Electron. https://doi.org/10.1109/tie.2021.3066926

27. Ning D, Du H, Zhang N, Jia Z, Li W, Wang Y (2021) A semiactive variable equivalent stiffness and inertance device implemented by an electrical network. Mech Syst Signal Process. https://doi.org/10.1016/j.ymssp.2021.107676

28. Li J-Y, Zhu S (2021) Tunable electromagnetic damper with synthetic impedance and self-powered functions. Mech Syst Signal Process. https://doi.org/10.1016/j.ymssp.2021.107822

29. Chen W (2007) Integrated control of automobile steering and suspension system based on disturbance suppression [J]. Chin J Mech Eng 43(11):98–104

30. Ning D, Du H, Sun S, Li W, Zhang B (2018) An innovative two-layer multiple-dof seat suspension for vehicle whole body vibration control. IEEE/ASME Trans Mechatron 23(4):1787–1799. https://doi.org/10.1109/tmech.2018.2837155

31. Ning D, Du H, Sun S, Li W, Zhang N, Dong M (2019) A novel electrical variable stiffness device for vehicle seat suspension control with mismatched disturbance compensation. IEEE/ASME Trans Mechatron 24(5):2019–2030. https://doi.org/10.1109/tmech.2019.2929543

32. Bai X-X, Cai F-L, Chen P (2019) Resistor-capacitor (RC) operator-based hysteresis model for magnetorheological (MR) dampers. Mech Syst Signal Process 117:157–169. https://doi.org/10.1016/j.ymssp.2018.07.050

33. Haiping D, Weihua L, Nong Z (2012) Integrated seat and suspension control for a quarter car with driver model. IEEE Trans Veh Technol 61(9):3893–3908. https://doi.org/10.1109/tvt.2012.2212472